

the plasma, the phase speed of the two frequency components are different. By tuning the amplitude of the two components, one can limit the K-shell ionization only occurring when the peaks of the two lasers overlap.

To understand this process, we first study the propagation of a bichromatic laser in plasmas. Consider two plane waves ($i = 1, 2$) with the normalized vector potentials

$$a_i(z, t) = a_{i0} \sin(\omega_i t - k_i z + \phi_i), \quad (1)$$

where a_{i0} are the amplitudes normalized to $m_e c^2/e$, ω_i are the frequencies, k_i are the wave numbers, ϕ_i are the initial phases of the two pulses, respectively. In the linear regime, their frequencies and wave numbers satisfy the linear dispersion relation $\omega_i^2 = \omega_p^2 + c^2 k_i^2$, and for low density plasmas the phase velocity can be expanded as $\frac{\omega_i}{k_i} = c(1 - \frac{1}{2}(\frac{\omega_p}{\omega_i})^2)^{-1}$, where $\frac{\omega_p}{\omega_i} \ll 1$. Substituting these expressions into Eq. (1), rewriting the variables using speed of light frame variables $\xi = \omega_1(t - \frac{z}{c})$ and $s = \frac{\omega_1}{c}z$, and normalizing the frequency to ω_1 , time to ω_1^{-1} , length to c/ω_1 , the laser vector potential can be rewritten as $a_1(\xi, s) = a_{10} \sin(\xi + \frac{1}{2}\omega_p^2 s + \phi_1)$ and $a_2(\xi, s) = a_{20} \sin(\omega_2 \xi + \frac{1}{2}\frac{\omega_p^2}{\omega_2} s + \phi_2)$. Correspondingly, the electric fields are normalized to $m_e \omega_i c/e$ and can be written as

$$\begin{aligned} E_1(\xi, s) &= a_{10} \cos(\xi + \frac{1}{2}\omega_p^2 s + \phi_1), \\ E_2(\xi, s) &= a_{20}\omega_2 \cos(\omega_2 \xi + \frac{1}{2}\frac{\omega_p^2}{\omega_2} s + \phi_2). \end{aligned} \quad (2)$$

The total electric field is given by $E(\xi, s) = E_1(\xi, s) + E_2(\xi, s)$. We choose $\omega_2 = 2$, $\omega_p = 0.01$ and $a_{20}/a_{10} = 1/4$ as an example, and the plot is shown in Fig. 2 (a). One can find out that changing ϕ_1 and ϕ_2 only leads to shifting the pattern in Fig. 2 (a) up and down (or left and right). The period of s over which the beat pattern changes is given by

$$\Delta s = \frac{4\pi}{\omega_p^2(\omega_2 - \frac{1}{\omega_2})}. \quad (3)$$

We only consider the situation that $a_{20} < a_{10}$ and ω_2 to be an integer larger than 1, and optimize the combination of a_{20}/a_{10} and ω_2 . Assume the peak field strength of $E(\xi, s)$ for a given s is $E_{\text{peak}}(s)$. Its maximum value is found at $s = s_1$ as $E_{\text{peak}|_{\text{max}}} = E_{\text{peak}}(s_1)$ and its minimum value is found at $s = s_2$ as $E_{\text{peak}|_{\text{min}}} = E_{\text{peak}}(s_2)$. Optimization for the controlled ionization injection can be realized by tuning the ratio

$$R(a_{20}/a_{10}, \omega_2) \equiv E_{\text{peak}|_{\text{max}}}/E_{\text{peak}|_{\text{min}}}. \quad (4)$$

It is easy to see that $E_{\text{peak}|_{\text{max}}} = a_{10} + a_{20}\omega_2$, but it is not straight forward to obtain $E_{\text{peak}|_{\text{min}}}$ analytically. From Eq. (2) one knows that the dispersion in plasma does not change $\langle E^2(\xi, s) \rangle$ (the power averaged over time ξ), though it changes the peak value of the bichromatic laser field. Consider a square wave at a particular value of s , which has the lowest peak amplitude for a given average power. As the laser evolves the average power remains a constant, but the superposition of the laser components will become narrower peaks

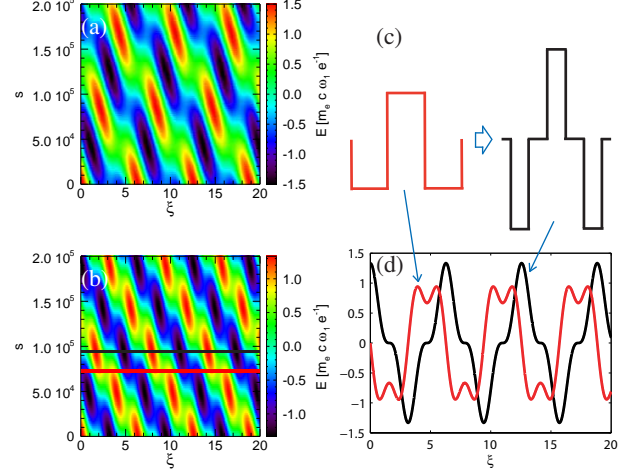


FIG. 2. (Color online) Typical evolution of the dual color lasers according to Eq. (2). (a) $a_{10} = 1$, $a_{20} = 1/4$, $\omega_2/\omega_1 = 2$ and $\omega_p/\omega_1 = 0.01$. (b) $a_{10} = 1$, $a_{20} = 1/9$, $\omega_2/\omega_1 = 3$ and $\omega_p/\omega_1 = 0.01$. (c) Illustration showing the reason to use a SWBL combination. (d) Two line-outs of (b) at s values indicated by the black and red lines.

as shown in Fig. 2 (c). A good approximation of a square wave is the first two components of its Fourier series, i. e., $\omega_2/\omega_1 = 3$ and $a_{20}/a_{10} = 1/9$ as shown in Fig. 2 (d). As one can see using only two frequencies approximates Fig. 2 (c) reasonably well. One can verify that the 1 : 3 combination is optimal by trying other combinations and compare the ratios defined by Eq. (4). We call this combination, the square-wave like bichromatic lasers (SWBL).

Based on the peculiar peak amplitude evolution of the SWBL, the ionization injection region can be broken into small pieces. By choosing the amplitude of the SWBL so that

$$E_{\text{peak}|_{\text{min}}} < E_{N^{5+}} < E_{\text{peak}|_{\text{max}}}, \quad (5)$$

the ionization injections can be limited to a few small separated regions, where $E_{N^{5+}}$ is the effective ionization threshold of N^{5+} . One may find $E_{\text{peak}|_{\text{max}}} = \frac{4}{3}a_{10}m_e c \omega_1 e^{-1}$ and $E_{\text{peak}|_{\text{min}}} = \frac{2\sqrt{2}}{3}a_{10}m_e c \omega_1 e^{-1}$.

In Fig. 3 we show the 1D PIC simulations results of such multiple ionization injection and acceleration process. ω_1 is chosen to be the frequency of the 800 nm laser and $a_{10} = 1.6$. The laser pulse duration is 33 fs in FWHM with the \sin^2 profile. The background plasma is provided by helium with the plasma density of $n_p = 1.6 \times 10^{-3}n_c$, where n_c is the critical density of the 800 nm laser. The injection provider is nitrogen with the density of $n_N = 1.6 \times 10^{-7}n_c$. The sequential ionization injections can be found in Fig. 3 (a). The curves in Fig. 3 (b) shows the evolution of the laser peak amplitude predicted by the theory and the result from the simulation. The differences of the theory and the simulation after some propagation distance are due to the plasma response and the nonlinear laser frequency shifting [39]. To control the injection bunch numbers we set the mixed gas length within an appropriate length of 1 mm. Such kind of gas jets have already been

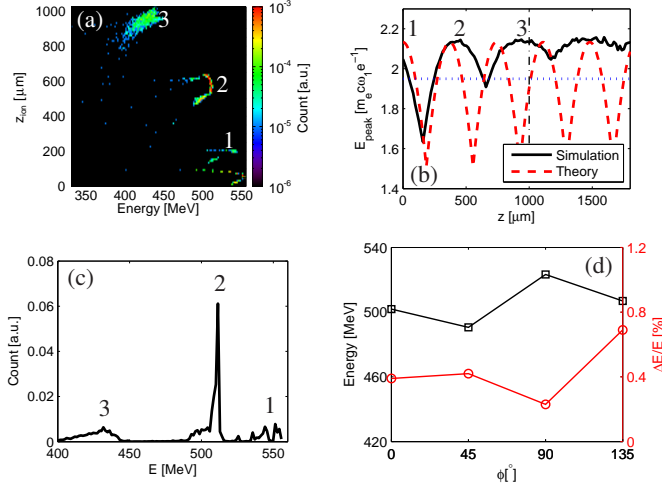


FIG. 3. (Color online) 1D PIC simulation of the SWBL and injections. (a) Electron energy at the diagnostic point vs. the initial position of the injected electrons. (b) The SWBL peak amplitude evolution. The blue dotted line is the estimated inner shell ionization threshold, and the black dash-dotted line is the separation from the mixed gas to the pure helium gas. (c) Electron beam spectrum at the distance $4860 \mu\text{m}$, where the minimum energy spread during the phase rotation is measured to be 0.29% in FWHM. (d) The energy and energy spread in FWHM vs. the initial laser phase ϕ .

used in several laboratories [32].

Totally three discrete bunches are observed in this simulation and the energy spectrum at an acceleration distance of $4854.4 \mu\text{m}$ is shown in Fig. 3 (c) with the three peaks labeled, corresponding to the three injections shown in Fig. 3 (a) and Fig. 3 (b) within the mixed gas region. Each injection duration is limited to $100 \sim 200 \mu\text{m}$. In this specific simulation, the second bunch has its minimal energy spread of 0.29% at distance of $4860 \mu\text{m}$, while the other two bunches can also get their minimum energy spreads at other appropriate acceleration distances. It is worth noting that even though the optimal acceleration distances for the minimal energy spreads are different for different bunches, this proposed scheme is robust because the accelerated beams can keep a low energy spread in a sufficient wide range of acceleration distances, which is clearer in multi-dimensional cases.

For such two color beat wave ionization injection scheme, the initial phases of the two pulses may affect the specific ionization injection position. Without loss of generality, let $\phi_1 = \phi_2 \equiv \phi$, and change ϕ from 0° to 135° , which correspondingly changes the positions of the electric field reaching $E_{\text{peak}|_{\text{max}}}$. The output beam energies and energy spreads at acceleration distance of $4800 \mu\text{m}$ are shown in Fig. 3 (d). One can see that the central energy of a specific electron bunch at a fixed laser propagation distance has a fluctuation of 30MeV, which is close to the energy difference between the first and second bunch shown in Fig. 3 (c). This energy fluctuation comes from the different injection positions set by the two laser phases. Nevertheless, we find all these simulations show

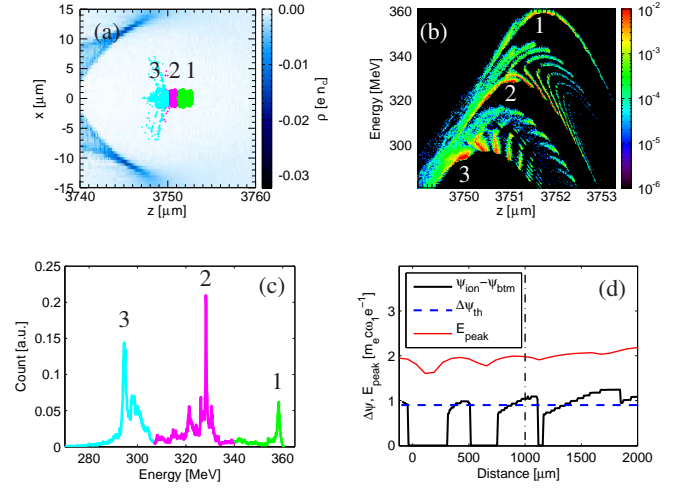


FIG. 4. (Color online) 2D PIC simulations of the SWBL injection scheme. (a) The density snapshot at $z = 3780 \mu\text{m}$. The colored dots show the locations of three electron bunches. (b) The energy and space distribution of the energetic electrons. (c) The spectrum of the injected electrons, showing three monoenergetic peaks. (d) The pseudo-potential (ψ) difference of the wake and the laser peak field evolution. The dash-dotted line is the separation from the mixed gas region to the pure helium region.

quite good beam quality. They keep small energy spreads of less than 1% regardless of the initial phase change.

Beside the phase effects, other high dimensional effects such as the self-focusing, the evolution of the bubble radius, and off axis ionizations, may also affect the injection and acceleration. Among them, self-focusing and the associated evolution of the bubble radius are most important. One of the solutions is to choose a matched spot size [38]. Another solution is to choose a relative large spot size so that self-focusing occurs after a sufficient long acceleration distance, during which multiple injections have already established. Generally, self-focusing occurs in a distance estimated by $z_{\text{sf}} = Z_R (\frac{\alpha}{32} a_0^2 k_p^2 W_0^2 - 1)^{-1/2}$, where $\alpha = \sqrt{2}$ for a 2D slab geometry and $\alpha = 1$ for a 2D cylindrical or 3D geometry [34, 40]. With the presence of self-focusing, a two-stage acceleration process should be deployed [31, 32]. For the multiple-injection to occur, it is required that the injection stage length satisfies

$$L_{\text{inj}} < z_{\text{sf}}. \quad (6)$$

In this case, the number of ionization injected bunches can be estimated as

$$N_{\text{bunch}} = \left\lfloor L_{\text{inj}} / \left(\frac{c\Delta s}{\omega_1} \right) \right\rfloor, \quad (7)$$

where the square brackets pair means the downward rounding. The energy difference between the monoenergetic peaks can be estimated by the injection position difference times the averaged acceleration gradient

$$\Delta \text{Energy} = \frac{c\Delta s}{\omega_1} \times \frac{1}{2} G_0, \quad (8)$$

where $G_0[\text{eV/m}] \approx 96 \sqrt{n_p[\text{cm}^{-3}]}$.

A typical 2D simulation is shown in Fig. 4, where we choose $a_{10} = 1.46$, $a_{20} = 0.162$, $W_0 = 80 \mu\text{m}$ and other parameters are the same as those in the 1D simulations. The initial laser amplitude in the 2D simulation is lower than that in 1D. But when the SWBL field reaches its first maximum in 2D, the peak field strength is very close to that in the 1D cases due to the self-focusing effect. The injection stage length is $L_{\text{inj}} = 1 \text{ mm}$ so that Eq. (6) is satisfied. A typical distribution of the injected bunches is shown in Fig. 4 (a). The central positions of these bunches are spatially separated at this snapshot with μm scale separations. Figure 4 (b) shows the phase space distribution of the bunches, from which we see within the second and the third bunches, there are a few micro bunches. These micro bunches come from the several overlapping peaks of the combined electric fields larger than the ionization threshold as schematically shown in Fig. 1. These bunches degrade the monochromaticity of the final beams, showing the pedestals between the peaks of the energy spectrum in Fig. 4 (c). In addition, the whole spectrum is composed of three main peaks with the separation of 30 MeV confirming the prediction of Eqs. (7) and (8). From our simulations we find these pedestals can be reduced by using a shorter 3ω laser, which makes the inner shell ionization only occurs in a single overlapping electric field peak. A simulation with 10 fs 3ω laser gives a single injected electron bunch with final energy spread less than 0.2% in FWHM.

The injection positions of the electrons can be estimated by evaluating both the ionization threshold and the pseudo-potential (ψ) differences [23] related to the wake and the ionized electrons. The threshold for ionization injection is given by $\Delta\psi_{\text{th}} = 1 - \frac{\sqrt{1+(p_{\perp}/m_e c)^2}}{\gamma_{\text{ph}}} \approx 0.9$, where the normalized transverse momentum is estimated to be the normalized laser vector potential at ionization $p_{\perp}/m_e c \approx 1.9$, and the wake phase velocity Lorentz factor is estimated by the linear theory $\gamma_{\text{ph}} \approx \omega/\omega_p = 25$. In Fig. 4 (d), the blue dashed line shows this threshold, and the black line shows the drop of ψ from the nitrogen K-shell ionization position to the minimum ψ , which is manually set to zero when the laser amplitude is lower than the K-shell ionization threshold. There are three periods in the injector region (distance up to 1000 μm) that satisfy the injection condition, consist with the three period when laser peak field exceeds the effective ionization threshold of the nitrogen inner shell, and also consist with the three injected bunches. In the simulation, we found that within a larger distance (between 3.5 mm and 4.5 mm), all of the bunches keep very low energy spread (less than 0.4% in FWHM). This gives a very larger acceleration distance window to get a high quality beam in experiments.

A series of 3D simulations are also performed. A typical result is shown in Fig. 5, in which we choose $n_p = 8 \times 10^{-4} n_c$, $a_{10} = 1.485$, $W_0 = 40 \mu\text{m}$ and $L_{\text{inj}} = 1 \text{ mm}$ so that $N_{\text{bunch}} = 1$ according to Eq. (7). A beam with a total charge of 12.6 pC, a mean energy of 389 MeV and a true RMS energy spread of 1.53% is produced, which confirms the effectiveness of

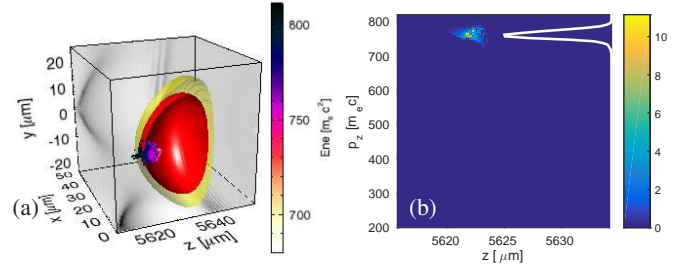


FIG. 5. (Color online) A 3D PIC simulation of the SWBL injections. (a) A 3D wake plot. Only a half of the bubble is plotted to show the inner structure of the bubble and the injected electrons. The electron beam has normalized emittances of $3.3 \mu\text{m} \cdot \text{rad}$ in the laser polarization direction, and $2.3 \mu\text{m} \cdot \text{rad}$ in the perpendicular direction. (b) Phase space of the injected charge. The white curve is the projection to the p_z axis.

SWBL injection scheme. From other 3D simulations we notice that as n_p decreases (laser power should be no less than the critical power for self-guiding while keeping a_0 unchanged, thus W_0 may be increased accordingly), the laser can be self-guided longer, the final electron beam energy increases, and the relative energy spread decreases. Although we have not yet tested the GeV level acceleration due to the limited computational resources available, from the serial 3D runs with absolute energy spread $\sim 5 \text{ MeV}$ it is very promising that our injection scheme can produce electron beams with energy spread lower than 1% once the plasma density and laser power are suitable for GeV level accelerations.

In conclusion, we have proposed a dual color laser scheme to control ionization injection in LWFAs. It can result in periodic triggering of the ionization injection and consequently produce a unique comb-like energy spectrum. These features are demonstrated by multi-dimensional PIC simulations. The energy spread of an individual electron bunch produced from a single injection period can be controlled down to around 1% or even less with the central energy of a few hundred MeV. Our scheme to generate multi-chromatic narrow energy-spread electron bunches can be used for multi color X-ray generation [4, 41], which is particularly interesting for medical imaging applications [42, 43]. The multi-chromatic beams may also be interesting for radiotherapy [44].

This work was supported by the National Basic Research Program of China (Grant No. 2013CBA01504), the National Natural Science Foundation of China (Grant Nos. 11421064, 11374209, 11374210 and 11405107), the MOST international collaboration project (Grant No. 2014DFG02330), the US DOE Grants No. DE-SC0008491, DE-SC0008316 and the US NSF Grant No. ACI-1339893. M.C. appreciates supports from National 1000 Youth Talent Project of China. The authors would like to acknowledge the OSIRIS Consortium, consisting of UCLA and IST (Lisbon, Portugal) for the use of OSIRIS and the visXD framework. Simulations were carried out on the II supercomputer at Shanghai Jiao Tong University.

* minchen@sjtu.edu.cn

† zmsheng@sjtu.edu.cn

- [1] T. Ishikawa *et al.*, *nature photonics* **6**, 540 (2012).
- [2] P. Emma *et al.*, *nature photonics* **4**, 641 (2010).
- [3] F. Krausz and M. Ivanov, *Rev. Mod. Phys.* **81**, 163 (2009).
- [4] T. Hara *et al.*, *Nat. Comm.* **4** (2013).
- [5] T. Tajima and J. M. Dawson, *Phys. Rev. Lett.* **43**, 267 (1979).
- [6] A. Oguchi *et al.*, *Physics of Plasmas* (1994-present) **15**, 043102 (2008).
- [7] S. Corde *et al.*, *Nat. Commun.* **4**, 1501 (2013).
- [8] O. Lundh, C. Rechatin, J. Lim, V. Malka, and J. Faure, *Phys. Rev. Lett.* **110**, 065005 (2013).
- [9] S. Chen *et al.*, *Phys. Rev. Lett.* **110**, 155003 (2013).
- [10] S. Cipiccia *et al.*, *Nat. Phys.* **7**, 867 (2011).
- [11] K. T. Phuoc *et al.*, *Nat. photonics* **6**, 308 (2012).
- [12] S. Corde *et al.*, *Rev. Mod. Phys.* **85**, 1 (2013).
- [13] W. Leemans *et al.*, *Nature physics* **2**, 696 (2006).
- [14] E. Esarey, C. B. Schroeder, and W. P. Leemans, *Rev. Mod. Phys.* **81**, 1229 (2009).
- [15] V. Malka, *Physics of Plasmas* (1994-present) **19**, 055501 (2012).
- [16] S. Hooker, *Nat. Photonics* **7**, 775 (2013).
- [17] X. Wang *et al.*, *Nature communications* **4** (2013).
- [18] K. Nakajima *et al.*, *Chin. Opt. Lett.* **11**, 013501 (2013).
- [19] X. Davoine, E. Lefebvre, C. Rechatin, J. Faure, and V. Malka, *Phys. Rev. Lett.* **102**, 065001 (2009).
- [20] M. Chen, Z.-M. Sheng, Y.-Y. Ma, and J. Zhang, *J. Appl. Phys.* **99**, 056109 (2006).
- [21] E. Oz *et al.*, *Phys. Rev. Lett.* **98**, 084801 (2007).
- [22] C. McGuffey *et al.*, *Phys. Rev. Lett.* **104**, 025004 (2010).
- [23] A. Pak *et al.*, *Phys. Rev. Lett.* **104**, 025003 (2010).
- [24] C. E. Clayton *et al.*, *Phys. Rev. Lett.* **105**, 105003 (2010).
- [25] B. Hidding *et al.*, *Phys. Rev. Lett.* **108**, 035001 (2012).
- [26] F. Li *et al.*, *Phys. Rev. Lett.* **111**, 015003 (2013).
- [27] N. Bourgeois, J. Cowley, and S. M. Hooker, *Phys. Rev. Lett.* **111**, 155004 (2013).
- [28] L.-L. Yu *et al.*, *Phys. Rev. Lett.* **112**, 125001 (2014).
- [29] X. L. Xu *et al.*, *Phys. Rev. ST Accel. Beams* **17**, 061301 (2014).
- [30] M. Chen *et al.*, *Phys. Rev. ST Accel. Beams* **17**, 051303 (2014).
- [31] B. B. Pollock *et al.*, *Phys. Rev. Lett.* **107**, 045001 (2011).
- [32] J. S. Liu *et al.*, *Phys. Rev. Lett.* **107**, 035001 (2011).
- [33] M. Chen, E. Esarey, C. B. Schroeder, C. G. R. Geddes, and W. P. Leemans, *Phys. Plasmas* **19**, 033101 (2012).
- [34] M. Zeng, M. Chen, Z.-M. Sheng, W. B. Mori, and J. Zhang, *Phys. Plasmas* **21**, 030701 (2014).
- [35] R. A. Fonseca *et al.*, *Lecture Notes in Computer Science*, Vol. 2331 (2002) pp. 342–351.
- [36] A. Pukhov and J. Meyer-ter Vehn, *Appl. Phys. B* **74**, 355 (2002).
- [37] W. Lu, C. Huang, M. Zhou, W. B. Mori, and T. Katsouleas, *Phys. Rev. Lett.* **96**, 165002 (2006).
- [38] W. Lu *et al.*, *Phys. Rev. ST Accel. Beams* **10**, 061301 (2007).
- [39] C. D. Murphy *et al.*, *Physics of Plasmas* (1994-present) **13**, 033108 (2006).
- [40] K.-C. Tzeng and W. B. Mori, *Phys. Rev. Lett.* **81**, 104 (1998).
- [41] A. Marinelli *et al.*, *Phys. Rev. Lett.* **111**, 134801 (2013).
- [42] C. Paulus *et al.*, *J. Instrument.* **8**, P04003 (2013).
- [43] B. Dierickx *et al.*, in *European Optical Society symposium, Munchen* (2009) pp. 16–18.
- [44] V. Malka *et al.*, *Nature Physics* **4**, 447 (2008).